Selection and characterization of anti-NF-κB p65 RNA aptamers

SUSAN E. WURSTER and L. JAMES MAHER III
Department of Biochemistry and Molecular Biology, College of Medicine, Mayo Clinic, Rochester, Minnesota, USA

ABSTRACT

NF-κB transcription factors include a group of five mammalian proteins that form hetero- or homodimers and regulate hundreds of target genes involved in acute inflammation, HIV-1 transcription activation, and resistance to cancer therapy. We previously used in vitro selection to develop a small RNA aptamer (anti-p50) that binds the DNA-binding domain of NF-κB $p50_2$ with low nanomolar affinity but does not bind NF-κB $p65_2$. Here, we report the in vitro selection of anti-NF-κB p65 RNA aptamers using parallel in vitro selections with either a fully randomized RNA library or a degenerate RNA library based on the primary sequence of the 31-nucleotide anti-p50 RNA aptamer. We report the characterization of these aptamers with respect to NF-κB target specificity, affinity, minimal sequence requirements, secondary structure, and competition with DNA κB sites. These results expand opportunities for artificial inhibition of NF-κB transcription factor dimers containing p65 subunits.

Keywords: NF-κB; aptamer; in vitro selection; p65

INTRODUCTION

NF-κB transcription factors regulate hundreds of genes whose products directly contribute to disease pathogenesis (Fujita et al. 1992; Verma et al. 1995; Chen and Ghosh 1999). Examples include cytokines such as TNFα, IL-6, IL-8, and INFγ as well as anti-apoptotic proteins such as c-IAPs, Bcl-2, and c-FLIP (Karin and Lin 2002; Dutta et al. 2006). Radiation, chemotherapeutic drugs, and biological agents (e.g., tumor necrosis factor [TNF]) act against tumor cells in part by triggering programmed cell death. However, this apoptotic response is commonly minimized by induction of stress-related gene expression through activation of NF-κB (Baeuerle and Baltimore 1996; Escarcega et al. 2007). Furthermore, NF-κB activation suppresses the ability of oncogenic *ras* mutations to stimulate apoptosis in tumor cells (Mayo et al. 1997). In contrast, inhibition of induced NF-κB has been shown to potentiate tumor cell killing by TNF, anticancer drugs, and radiation (Beg and Baltimore 1996). The potential therapeutic value of inhibiting NF-κB in tumor cells has been emphasized (Baldwin 1996; Lin and Karin 2003; Nakanishi and Toi 2005) and is suggested by the antitumor effects of antisense oligonucleotides targeting NF-κB in tissue culture and animal models (Kitajima et al. 1992).

Studies have also highlighted the potential contribution of NF-κB-mediated inflammation to cancer progression (Karin and Lin 2002; Karin et al. 2002; Dobrovolskaia and Kozlov 2005; Karin and Greten 2005). It is estimated that 15% of cancers coincide with the presence of infection (Dobrovolskaia and Kozlov 2005). NF-κB may play a role in linking inflammatory responses and the growth of malignant cells (Perwez Hussain and Harris 2007; Van Waes 2007). Immune cells stimulated by invading pathogens such as bacteria or viruses produce inflammatory cytokines and chemokines via NF-κB activation. Released cytokines and chemokines then further stimulate the NF-κB pathway in neighboring cells. If local transformed cells are stimulated, NF-κB may promote transcription of genes that allow cells to evade apoptosis and bypass cell cycle checkpoints.

Because of its prominent roles in inflammation, cancer, and HIV-1 activation (Suzan et al. 1991; Garg and Aggarwal 2002; Karin and Greten 2005; Karin 2006), NF-κB proteins are attractive targets for therapeutic inhibition. As DNA-binding proteins, NF-κB family members have a natural affinity for nucleic acids (Chen et al. 1998). We have been interested in using in vitro selection methods (Ellington and Szostak 1990; Tuerk and Gold 1990; Burke and Berzal-Herranz 1993; Burke et al. 1996) to develop RNA decoy molecules for the direct inhibition of subunits

Reprint requests to: L. James Maher III, Department of Biochemistry and Molecular Biology, 200 First Street SW, Rochester, MN 55905, USA; e-mail: maher@mayo.edu; fax: (507) 284-2053.

Article published online ahead of print. Article and publication date are at http://www.rnajournal.org/cgi/doi/10.1261/rna.878908.

of the classical NF-κB heterodimer, p50 and p65 (Cassiday and Maher 2002). Developing RNA aptamers to NF-κB affords the opportunity to express inhibitors from transgenes with the goal of artificial gene regulation.

Previously, we selected and characterized an anti-p50 RNA aptamer that binds to the p50 subunit of NF-κB. This RNA decoy was characterized both in vitro and in *Saccharomyces cerevisiae* (Lebruska and Maher 1999; Cassiday and Maher 2001, 2003; Cassiday et al. 2002) and the X-ray crystal structure of the anti-p50/$p50_2$ complex was determined (Huang et al. 2003). The solution structure of the unbound anti-p50 RNA aptamer has also recently been determined, showing the RNA to be highly prestructured in the absence of protein (Reiter et al. 2008). These structural studies indicate that the anti-p50 RNA is remarkable in its mimicry of the κB consensus DNA binding site. The aptamer contacts the same amino acids involved in DNA base-specific recognition (Huang et al. 2003; Hayden and Ghosh 2004). Interestingly, adenoviral-mediated transduction of the anti-p50 aptamer into A549-derived tumors in a murine model suggests that this RNA significantly delays tumor growth (Mi et al. 2006). These authors further report that anti-p50 blocks the ability of activated NF-κB to directly or indirectly regulate genes such as Bcl-xL, HIF-1α, eNOS, and VEGF (Mi et al. 2006). These studies again highlight the therapeutic potential of anti-NF-κB RNA aptamers.

Unlike p65, NF-κB p50 does not contain a C-terminal transactivation domain (Ghosh et al. 1995), and recent reports suggest that a $p50_2$/Bcl-3 complex acts as a repressor by competing with p50/p65 heterodimers and p65 homodimers for binding to consensus κB DNA sites (Carmody et al. 2007). Thus, aptamer inhibition of the $p50_2$ form of NF-κB might be expected to *increase* gene activation by $p65_2$ in some contexts. In contrast, siRNA-mediated knockdown of the p65 subunit leads to sensitization of cancer cells to chemotherapeutic agents (Guo et al. 2004). We therefore initiated in vitro selections to identify p65-specific RNA aptamers.

Figure 1A depicts a sequence alignment of the DNA-binding amino acids of p50 and p65 located in loop L1 (Huang et al. 2003; Hayden and Ghosh 2004) with amino acids critical for specific nucleic acid recognition indicated. Five of seven p65 residues involved in DNA recognition are conserved in p50 (Fig. 1A, circles). The $p50_2$ transcription factor dimer forms a "closed" complex around the DNA duplex (Fig. 1B, left). However, when anti-p50 RNA aptamers saturate both p50 subunits, the protein dimer adopts a nonnative, "open" conformation (Fig. 1B, right; Huang et al. 2003). The anti-p50 RNA aptamer contacts essentially the same amino acids involved in DNA recognition by p50 (Fig. 1A, squares). Despite the sequence similarity between p50 and p65, the anti-p50 RNA aptamer displays remarkable specificity for p50, with an affinity for the p65 subunit that is orders of magnitude lower (Huang et al. 2003). Based on previous crystallographic studies

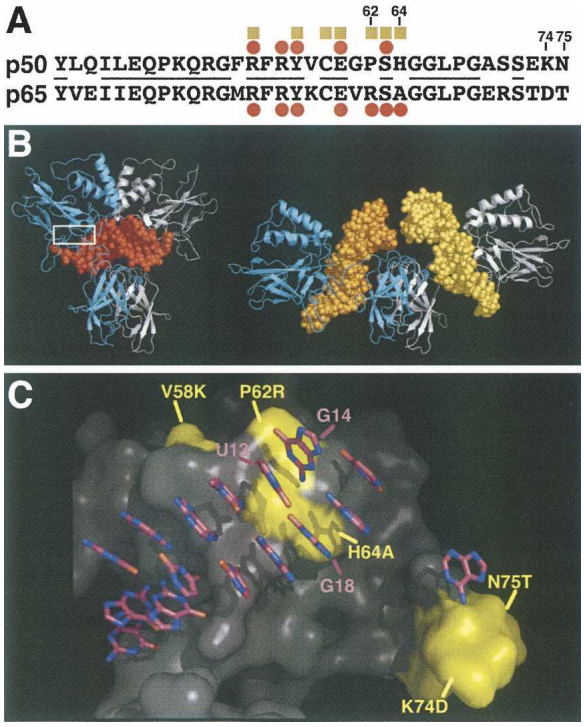

FIGURE 1. NF-κB p50 and p65 nucleic acid recognition. (*A*) Sequence alignment of NF-κB p50 and p65 loop L1 amino acids necessary for nucleic acid recognition. Identical amino acids are underlined. Loop L1 amino acids responsible for DNA base-specific contacts in p50 and p65 (red circles) are generally conserved and are similar to those making base-specific contacts with the previously selected anti-p50 RNA aptamer (gold squares). (*B*, *Left*) $p50_2$ (cyan and gray) binding κB DNA (red). Box indicates position of loop L1. (*Right*) Two copies of the previously selected anti-p50 RNA aptamer (shades of gold) bind $p50_2$ (cyan and gray) in a nonnative, "open" conformation with the RNA contacting the DNA-binding amino acids of $p50_2$. (*C*) Differences between p50 (gray) and p65 (yellow) amino acids mapped onto the anti-p50 RNA aptamer contact surface of p50 as based on previous crystallogaphic studies (PDB accession 1ooa). Aptamer bases are rendered in pink and blue.

(Huang et al. 2003), Figure 1C depicts anti-p50 nucleotides (nt) (pink/blue) mapped onto the surface of the p50 subunit (gray). Amino acids that differ between p50 and p65 are highlighted in yellow.

In an attempt to alter the specificity of anti-p50 RNA aptamers to target $p65_2$, we performed in vitro selections of anti-p65 RNA aptamers using two different RNA libraries. One library contained 60 random nucleotides. A second "degenerate" library was based on the original anti-p50 aptamer with 9% mutation frequency at each position. Here, we characterize anti-p65 RNA aptamers selected from both libraries.

RESULTS AND DISCUSSION

R1, R2, and D1 RNA aptamers are ligands for $p65_2$

We identified high-affinity RNA aptamers for $p65_2$ using cycles of in vitro affinity selection and amplification. The

initial fully-randomized library represented $\sim 10^{14}$ different sequences with 60 random nucleotides flanked by constant termini allowing for reverse transcription and PCR amplification. A secondary degenerate library was based on the primary sequence of the anti-p50 aptamer. Twelve cycles of parallel selections were performed, and the resulting selected RNAs were cloned and sequenced. Figure 2A compares the predicted secondary structure of the aptamers selected against p65, the previously selected anti-p50 aptamer, and a scrambled RNA control (Scr). The fully random RNA library gave rise to two dominant sequences: R1 (10 of the 30 sequenced clones) and R2 (4 of the 30 sequenced clones). Sixteen other clones shared no homology with one another or with R1 or R2 (not shown). The degenerate RNA library gave rise to a single dominant sequence termed D1. In comparison to the sequence of anti-p50, D1 contains 8 nt changes (Fig. 2A, triangles). Secondary structures of R1, R2, and D1 were predicted by conventional computational methods (Jaeger et al. 1989, 1990; Zuker 1989). R1 is predicted to form a central, small hairpin loop with an asymmetric internal bulge (Fig. 2A). RNAs R2 and D1 are also predicted to form imperfect hairpins (Fig. 2A).

Equilibrium dissociation constants for R1, R2, and D1 with either $p65_2$ or $p50_2$ proteins were estimated and compared to control anti-p50 and scrambled RNAs by both nitrocellulose filter binding assays and electrophoetic gel mobility shift assays in order to provide two independent measurements of K_d (Fig. 2B–D; Table 1). Care was taken to show that the K_d estimates were independent of the concentration of radiolabeled aptamer, confirming that pseudo-first-order kinetics applied (data not shown). Electrophoretic gel mobility shift experiments gave no evidence for higher-order complexes over the linear portions of the binding curves (Fig. 2D). Both R1 and R2 RNA aptamers displayed high affinity for $p65_2$, with measured dissociation constants in the 10–40 nM range. Strikingly,

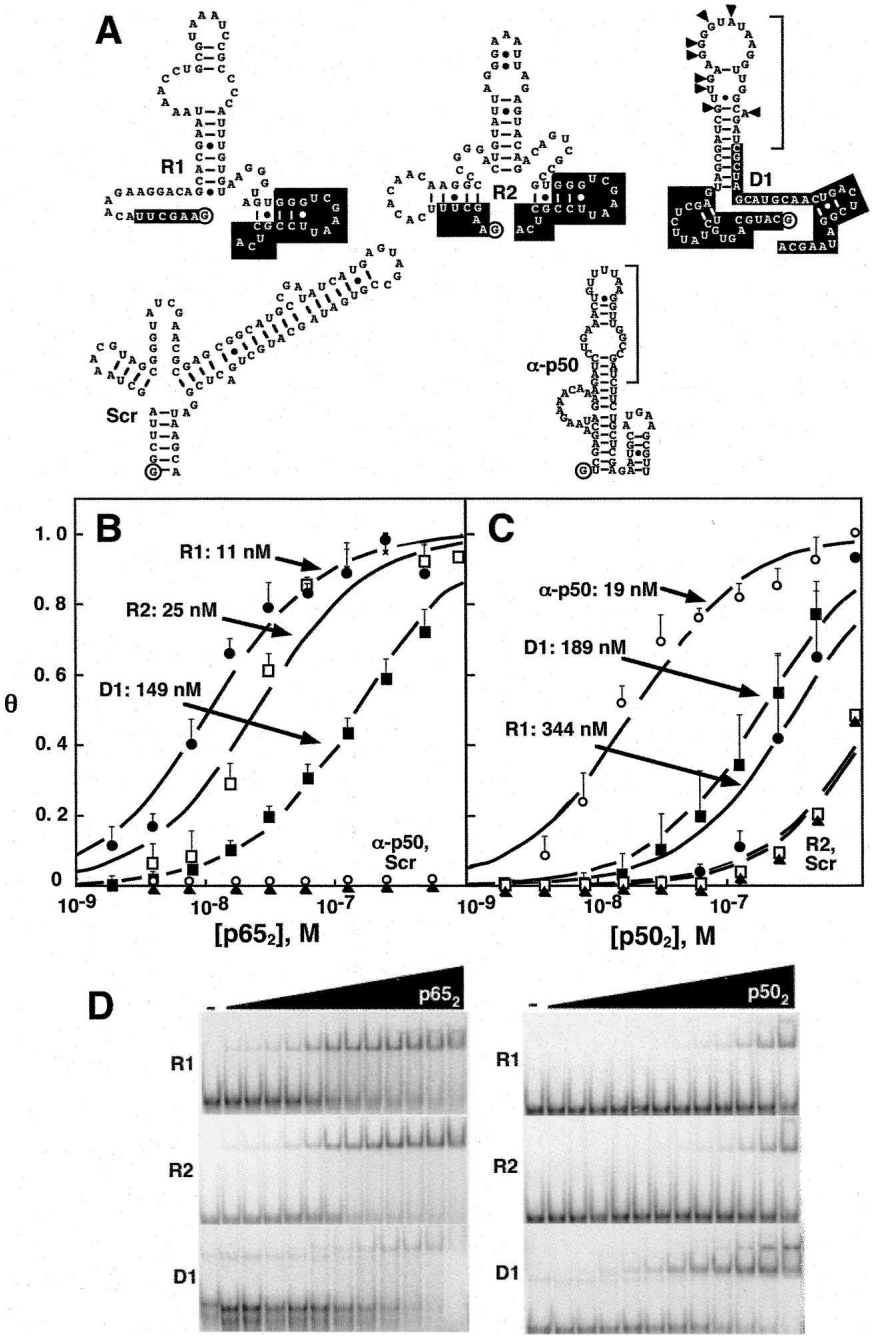

FIGURE 2. RNA aptamer binding affinities for $p50_2$ and $p65_2$ forms of NF-κB. (*A*) Predicted RNA secondary structures of R1, R2, D1, Scr, and anti-p50. 5′ and 3′ constant regions retained from the initial library selections (R1) or nucleotides that were not degenerate (D1) are in white. The 5′ terminal nucleotide is circled. Brackets indicate the minimal anti-p50 RNA or derived aptamer sequences. Anti-p65 D1 changes (relative to anti-p50) are indicated with triangles. (*B*) Binding isotherms fit to data averages for RNA aptamer complexes with $p65_2$ (n = 3). Error bars represent the standard error of the mean. (R1) filled circles; (R2) open squares; (D1) filled squares; (anti-p50) open circles; (Scr) filled triangles. (*C*) Average binding isotherms for RNA aptamer complexes with $p50_2$ (n = 3). Error bars represent the standard error of the mean. Symbols are as in panel *B*. (*D*) Representative electrophoretic gel mobility shift experiments for RNA aptamer complexes with $p65_2$ (*left*) and $p50_2$ (*right*). Protein concentrations range from 0.6 nM to 512 nM.

TABLE 1. Characterization of anti-p65 RNA aptamer specificity and affinity for NF-κB proteins

Aptamer	K_d ($p65_2$) (nM)[a]	K_d ($p65_2$) (nM)[b]	K_d ($p50_2$) (nM)[a]	K_d ($p50_2$) (nM)[b]
R1	11 ± 2	26 ± 14	344 ± 200	560 ± 120
R2	25 ± 10	10 ± 2	1556 ± 300	990 ± 155
D1	149 ± 51	206 ± 141	190 ± 92	68 ± 17
Anti-p50	>>5000	>>5000	20 ± 4	10 ± 2
Scr	>>5000	1132 ± 78	1506 ± 290	548 ± 34

[a]Equilibrium dissociation constant from nitrocellulose filter binding data fit to Equation 1. Mean and standard deviation are shown based on at least three repeats.
[b]Equilibrium dissociation constant from electrophoretic gel mobility shift experiments fit to Equation 1. Mean and standard deviation are shown based on at least two repeats.

neither R1 nor R2 displayed high affinity for $p50_2$. In contrast, the D1 RNA aptamer displayed moderate affinity for both $p65_2$ and $p50_2$ (dissociation constants of 50–300 nM). Thus, these selections yielded both RNA aptamers with high affinity and selectivity for $p65_2$ (R1 and R2) and an RNA aptamer of moderate affinity for both $p65_2$ and $p50_2$ (D1).

While equilibrium dissociation constants for the binding of aptamers R1 and R2 to $p65_2$ are within one order of magnitude, data from filter binding experiments indicate that R1 RNA binds more tightly while quantification of electrophoretic gel mobility shift experiments suggests that R2 is the higher affinity aptamer (Fig. 2B,D; Table 1). To directly compare the affinities of these two RNAs, we performed RNA binding competition experiments in which radiolabeled R1 or R2 was incubated with different concentrations of unlabeled competitor RNA in the presence of limiting $p65_2$. Figure 3A shows the result of such an experiment using an electrophoretic mobility shift assay with radiolabeled R1 RNA incubated in the presence of $p65_2$ alone (Fig. 3A, lane 2) or increasing molar excess concentrations of unlabeled R1 (Fig. 3A, lanes 3–5), unlabeled scrambled RNA (Fig. 3A, lanes 6–8), unlabeled R2 RNA (Fig. 3A, lanes 9–11), or unlabeled D1 RNA (Fig. 3A, lanes 12–14). Based on quantitation of shifted and unshifted bands, unlabeled R1 RNA was observed to most effectively compete with labeled R1 RNA for binding to $p65_2$. Unlabeled R2 RNA was less effective in competition. The converse experiment was also performed (Fig. 3B). In agreement with the previous results, labeled R2 RNA did not effectively compete with unlabeled R1 for binding to $p65_2$ (Fig. 3B, lanes 9–11). Importantly, the observed competition for binding to $p65_2$, rather than formation of a new complex of lower electrophoretic mobility, suggests that R1 and R2 compete for overlapping binding sites on $p65_2$. It is also formally possible that a conformational change induced by binding one RNA precludes a second RNA binding at a different site or induces an unstable triple complex. Further studies were focused on characterizing the anti-p65 R1 RNA.

R1 RNA binds $p65_2$ with a 1:1 stoichiometry

Electrophoretic gel mobility shift experiments (e.g., Fig. 2D; Table 1) showed only a single $p65_2$:R1 complex under the conditions of protein excess used to estimate equilibrium dissociation constants. Thus, there is no evidence for the binding of multiple p65 dimers per RNA. To explore the stoichiometry under conditions of RNA excess we employed a titration analysis. We incubated a constant concentration of $p65_2$ protein (50 nM; greater than the K_d for binding R1) with increasing concentrations of radiolabeled R1 RNA. The concentration of R1 RNA relative to $p65_2$ ranged from 0.1 to 3 such that RNA

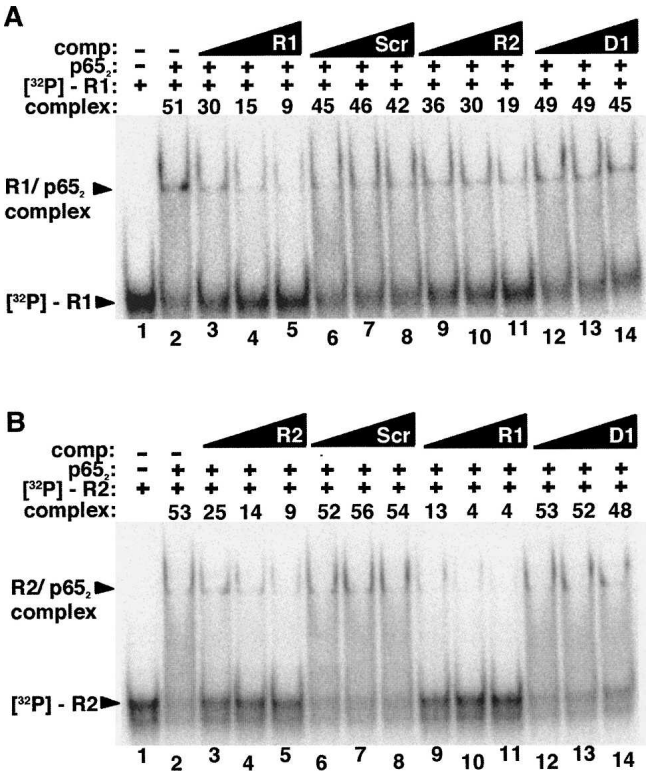

FIGURE 3. RNA competition binding assay comparing $p65_2$ affinity for RNAs R1 and R2. (*A*) Labeled R1 RNA (1 nM) was incubated in the absence of protein (lane *1*) or the presence of $p65_2$ alone (20 nM) (lane *2*) or together with various unlabeled RNA competitors (lanes *3–14*): R1 RNA (lanes *3–5*), 83 nt scrambled RNA (lanes *6–8*), R2 RNA (lanes *9–11*), D1 RNA (lanes *12–14*). Triangles indicate increasing unlabeled RNA competitor concentration (one-, two-, or fourfold molar excess [20 nM, 40 nM, or 80 nM] relative to $p65_2$ concentration). "Complex" indicates the percentage of radiolabeled probe shifted. (*B*) As in *A*, except radiolabeled R2 RNA was tested and lanes *3–5* and *9–11* are in the presence of R2 and R1 competitor, respectively.

binding will saturate the protein. The results are shown in Figure 4. As RNA concentration increases, the $p65_2$/R1 complex appears as a single species (Fig. 4, cf. lanes 1 and 2). This single species persists with increasing RNA concentration and there is no appearance of additional complexes (Fig. 4, cf. lanes 2–7). Thus, even when the R1 aptamer concentration is threefold higher than the concentration of $p65_2$, there is no evidence for the formation of a $p65_2$:$R1_2$ complex. This result indicates that the $p65_2$:R1 stoichiometry is 1:1.

Truncation analysis of R1 RNA

We wished to determine the minimal region of the R1 aptamer necessary and sufficient for high affinity binding to $p65_2$. Initially, boundary assay experiments were performed by radiolabeling either 5′ or 3′ R1 termini, performing limited base hydrolysis, and selecting radiolabeled fragments competent to bind $p65_2$. Unexpectedly, the corresponding minimal R1 sequence obtained by simultaneous truncation of both termini of R1 did not tightly bind $p65_2$ (data not shown). Therefore, we undertook systematic R1 truncations (Fig. 5A). First, we created aptamer R1-1 by deletion of the indicated nucleotides in the 5′ and 3′ constant regions (white lettering) of R1 (Fig. 5A). The affinity of R1-1 for $p65_2$ was reduced to 125 nM compared to 11 nM for R1. Other data (not shown) suggested that a G_3 trinucleotide in the 3′ constant region of R1 (Fig. 5A, horizontal bar) is required for high affinity binding to $p65_2$. We then tested RNAs in which this trinucleotide was preserved but the 5′ terminus of the R1-1 RNA was systematically truncated (Fig. 5, R1-1a, R1-1b, R1-1c). As shown in Figure 5B, progressive deletion of 5′ sequences caused up to 40-fold reduction in $p65_2$ affinity. This analysis suggests that R1 binding to p65 involves structures beyond the predicted central hairpin and bulged loop. This result distinguishes R1 RNA binding to $p65_2$ from anti-p50 RNA binding to $p50_2$, where the latter aptamer retains high target affinity even when truncated to 29 nt (Cassiday and Maher 2002).

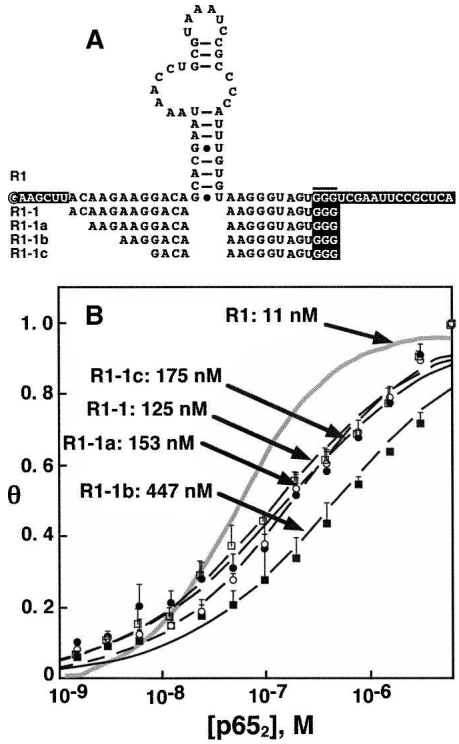

FIGURE 5. $p65_2$ binding by R1 truncations. (*A*) R1 terminal truncation series. The 5′ terminus of R1 is circled and fixed terminal sequences are shown in white lettering. The G_3 trinucleotide important for high-affinity binding is indicated by a horizontal bar. (*B*) Average binding isotherms based on electrophoretic gel mobility shift experiments. Error bars represent the standard error of the mean. Fit values of K_d are shown for indicated R1 truncations. Gray trace corresponds to apamer R1.

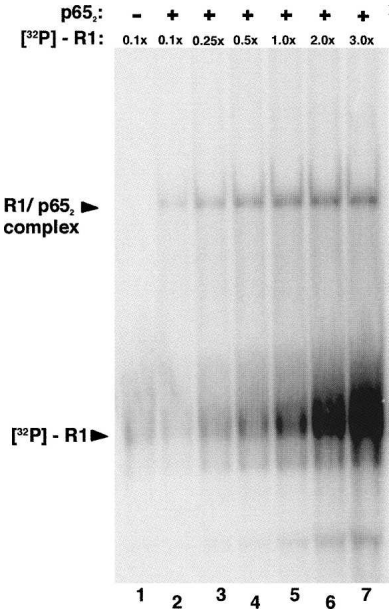

FIGURE 4. R1 RNA binds $p65_2$ with a 1:1 stoichiometry. R1 RNA titration strategy to determine the stoichiometry of the $p65_2$/R1 RNA complex. Labeled R1 RNA was incubated alone (lane *1*) or in the indicated increasing concentrations relative to $p65_2$ (50 nM) (lanes *2–7*).

Characterization of R1 RNA folding

Because the truncation analysis of R1 suggested the importance of sequence outside the predicted bulged stem–loop, we sought additional information about the secondary structure of R1. RNAs D1 and anti-p50 were included for comparison. We used partial digestion with RNase V_1 and mung bean nuclease to assess base pairing and compared cleavage patterns with G-specific RNase T_1 ladders (Fig. 6). RNase V_1 is a ribonuclease that detects both double-stranded and stacked single-stranded regions (Brown and Bevilacqua 2005). Mung bean nuclease preferentially attacks single-stranded nucleic acids. Anti-p50

structural data suggest that the 29-nt anti-p50 RNA includes two double-stranded helical segments that flank an internal bulge with stacked nucleotides (Huang et al. 2003; Reiter et al. 2008). Indeed, the anti-p50 RNA was cleaved by the double-strand-specific RNase V_1 throughout the flanking duplexes and internal bulge (Fig. 6, right, squares). Mung bean nuclease digestion of anti-p50 RNA showed preferential sensitivity in the terminal loop, whereas the flanking duplexes were more protected (Fig. 6, cf. lanes 4 and 5, and map at right). The secondary structure prediction for R1 suggests that the folded RNA includes a central hairpin with an asymmetric internal loop (Fig. 6, right). RNase V_1 produced strong and weak cleavage at nucleotides throughout this predicted central hairpin region. This result suggests that most of this hairpin and asymmetric bulge contain double-stranded or stacked segments of nucleotides. Interestingly, the 3′ portion of R1 (nucleotides 49–81), which contains G67–G69 that are important for $p65_2$ binding, resisted RNase V_1 attack but displayed a complementary strong mung bean nuclease cleavage pattern (Fig. 6, cf. lanes 9 and 10). In order to better elucidate the structure of R1 near the 5′ terminus, we labeled the 3′ terminus of the molecule and repeated the analysis (Fig. 6, lanes 11–15). The 5′-terminal region of R1 is largely susceptible to mung bean nuclease cleavage. The only indication that base pairing or base stacking may be present near the 5′ terminus of the molecule is provided by moderate RNase V_1 cleavage at nucleotides 16–19 (Fig. 6, cf. lanes 14 and 15). Taken together, these results suggest that both the 5′ and 3′ terminal regions of R1 may be single stranded and flexible in solution. Nuclease analysis of D1 suggests a double-stranded region of RNA that matched the predicted central hairpin. Terminal loop nucleotides appear to be unpaired and accessible to mung bean nuclease, as do the 3′ terminal nucleotides of the molecule (Fig. 6, cf. lanes 19 and 20, and map at right).

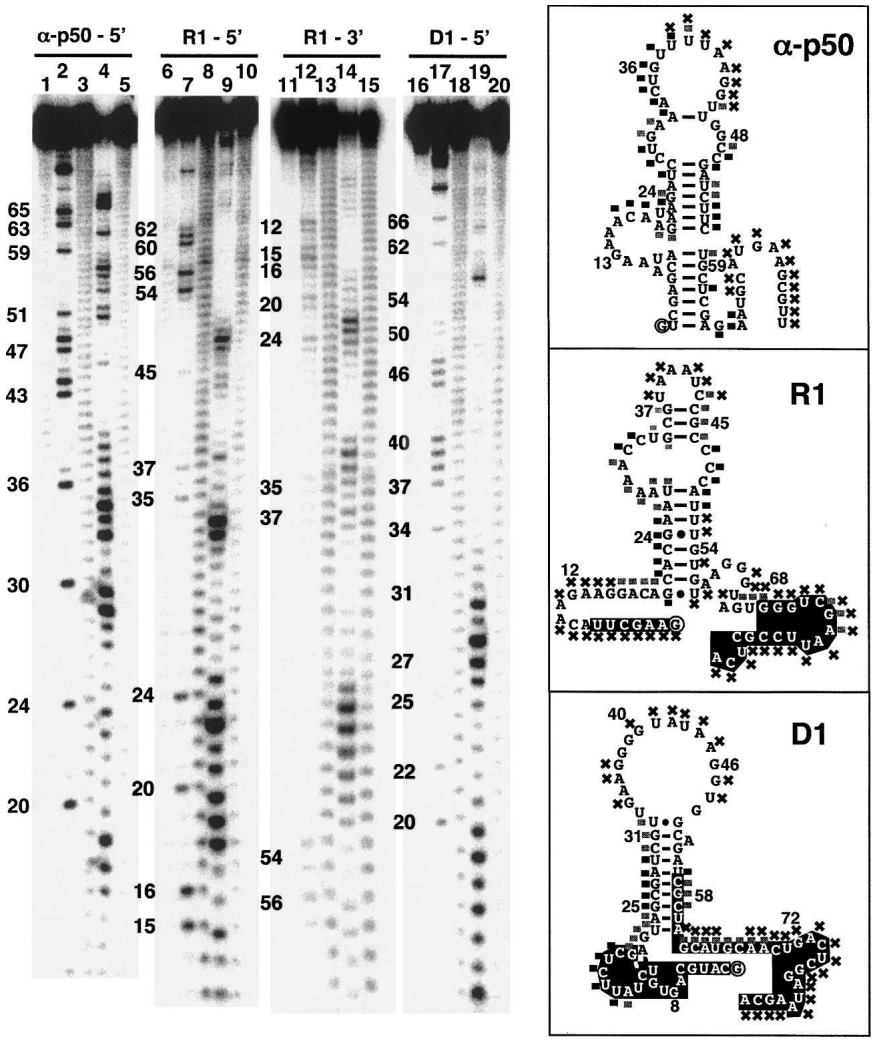

FIGURE 6. Structural characteristics of anti-NF-κB RNA aptamers by RNase probing. Analysis of anti-p50 (lanes *1–5*), R1 (lanes *6–15*), and D1 (lanes *16–20*). Labeled RNA aptamers were incubated alone (lanes *1*, *6*, *11*, and 16), in the presence of RNase T1 (lanes *2*,*7*,*12*,*17*), elevated pH (lanes *3*,*8*,*13*,*18*), RNase V_1 (lanes *4*,*9*,*14*,*19*), or mung bean nuclease (lanes *5*,*10*,*15*,*20*). RNase V_1 cleavage products include a 3′ terminal phosphate, which consistently retards migration of the RNA fragments by the equivalent of 0.5 nt in comparison to RNase T_1 and alkaline hydrolysis ladders that terminate in a 3′ hydroxyl residue (Brown and Bevilacqua 2005). Cleavage patterns were qualitatively mapped onto predicted RNA secondary structures shown at *right*. Black and gray squares indicate accessible and partially accessible sites, respectively, for RNase V_1 cleavage. Sites accessible to mung bean nuclease as indicated (X). 5′ and 3′ constant regions retained from the initial library selections (R1) or nucleotides that were not degenerate (D1) are in white.

Anti-p65 R1 RNA 3′ terminal sequences are important for high $p65_2$ affinity

Truncation analyses (Fig. 5) highlighted the importance of R1 3′ terminal sequences for high-affinity $p65_2$ binding. We were interested in determining if R1 3′ nucleotides are required for base-specific contacts with $p65_2$ or if these nucleotides play a nonspecific, perhaps electrostatic role. We prepared R1 aptamer variants with two alternative 3′ sequences (Fig. 7A). In one case, the 3′ sequence of R1 (Fig. 7A, top) was modified by substitution of the important G_3 trinucleotide (nucleotides 67–69) in the 3′ sequence of R1 with an A_3 sequence to produce aptamer R1 G(67–69)A

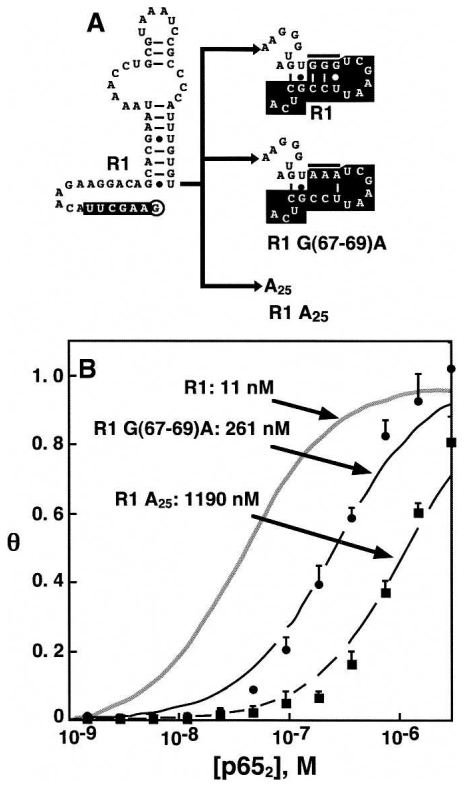

FIGURE 7. Anti-p65 R1 RNA 3′ terminal tail is required for high $p65_2$ affinity. (*A*) 3′ terminal nucleotides of R1 RNA (*top*) were altered by either substitution of three adenines at positions 67–69 (*middle*, compare to horizontal bar at *top*) or replacement by the sequence A_{25} (*bottom*). Constant regions retained from initial selections are lettered in white. (*B*) Labeled R1 RNA and 3′ substituted forms of R1 RNA were used in electrophoretic gel mobility shift experiments with $p65_2$ ($n = 2$). Quantitation resulted in average binding isotherms shown in the figure, with error bars representing the standard error of the mean.

(Fig. 7A, middle). In the second case, the final 25 nt of R1 were replaced by A_{25} to produce aptamer R1 A_{25} (Fig. 7A, bottom). Binding isotherms for these aptamer variants are shown in Figure 7B. The data reveal that perturbation of R1 3′ sequences severely reduces affinity for $p65_2$. This result shows that R1 3′ sequences are participating in base-specific contacts with $p65_2$.

R1 and D1 RNA aptamers as "decoys" for NF-κB

Previously, we identified an anti-p50 RNA aptamer and showed that it competes with κB DNA for $p50_2$ protein binding in vitro and in vivo (Lebruska and Maher 1999; Cassiday and Maher 2002). We therefore used competition gel mobility shift experiments to test the ability of anti-p65 RNA aptamers R1 and D1 to compete with κB DNA for binding to $p65_2$ in head-to-head competitions (Fig. 8A,B), or in the presence of preformed DNA/protein complexes (Fig. 8B). As a comparison, we measured an equilibrium dissociation constant of 7 ± 2 nM for the κB DNA/$p65_2$ complex (data not shown). In panel A, radiolabeled κB DNA was incubated in the absence of $p65_2$ (Fig. 8A, lanes 1 and 15), in the presence of $p65_2$ alone (Fig. 8A, lane 2) or together with various unlabeled competitors: κB DNA (Fig. 8A, lanes 3–5), nonspecific DNA (Fig. 8A, lanes 6–8), scrambled RNA (Fig. 8A, Scr: lanes 9–11), R1 RNA (Fig. 8A, lanes 12–14), R1–7 RNA (Fig. 8A, lanes 16–18), and D1 RNA (Fig. 8A, lanes 19–21). Triangles indicate increasing unlabeled competitor nucleic acid concentration: three-, six-, or ninefold molar excess (Fig. 8A, lanes 3–14) or 50-, 100-, or 500-fold molar excess (Fig. 8A, lanes 16–21) relative to $p65_2$. The quantified results indicate that full-length R1 RNA effectively competes with κB DNA for binding to $p65_2$ in head-to-head competition (Fig. 8A, lanes 12–14). R1–7 and D1 also compete with κB DNA for binding to $p65_2$, although less effectively than R1 (Fig. 8A, lanes 15–21). The observation that anti-p65 RNA aptamers R1, R1-7, and D1 compete with κB DNA for $p65_2$ binding suggests that, like anti-p50, the binding site of these RNA aptamers overlaps with the electrostatically favorable DNA-binding domain of p65. In panel B, radiolabeled κB DNA was incubated in the absence of $p65_2$ (Fig. 8B, lane 1), in the presence of $p65_2$ alone (Fig. 8B, lane 2), together in head-to-head competition with three- or sixfold molar excess unlabeled RNAs (Fig. 8B, lanes 3–4,7–8,11–12) or preincubated with $p65_2$ to achieve the formation of preformed DNA/ protein complexes (Fig. 8B, lanes 5–6,9–10,13–14). The ability of the unlabeled competitor RNAs to disrupt the preformed complexes was compared. The result suggests that unlabeled competitor RNA is equally effective at competing for binding to $p65_2$ in both head-to-head competitions and in the presence of preformed complexes.

Summary and future prospects

In the present study, we selected high affinity RNA aptamers that appear to target the DNA-binding domain of the transcription factor NF-κB p65 subunit. These selection results provide additional support for the hypothesis that RNA ligands can target the nucleic acid binding surface of DNA-binding proteins such as transcription factors. The prototypical example is the *Xenopus* transcription factor TFIIIA (Cassiday and Maher 2002). When DNA-binding proteins are the target of RNA selection, the DNA-binding domain tends to be included in the preferred RNA binding site (Lebruska and Maher 1999; Cassiday and Maher 2001; Huang et al. 2003; Choi et al. 2006; Zhao et al. 2006). Thus, transcription factors implicated in disease pathogenesis may be exploited for the development of therapeutic nucleic acid inhibitors such as RNA aptamers.

We have now reported RNA aptamers specific for either the p50 or p65 subunit of the classical NF-κB heterodimer. The aptamers are surprisingly different, and approaches to convert anti-p50 to an anti-p65 RNA by a small number of

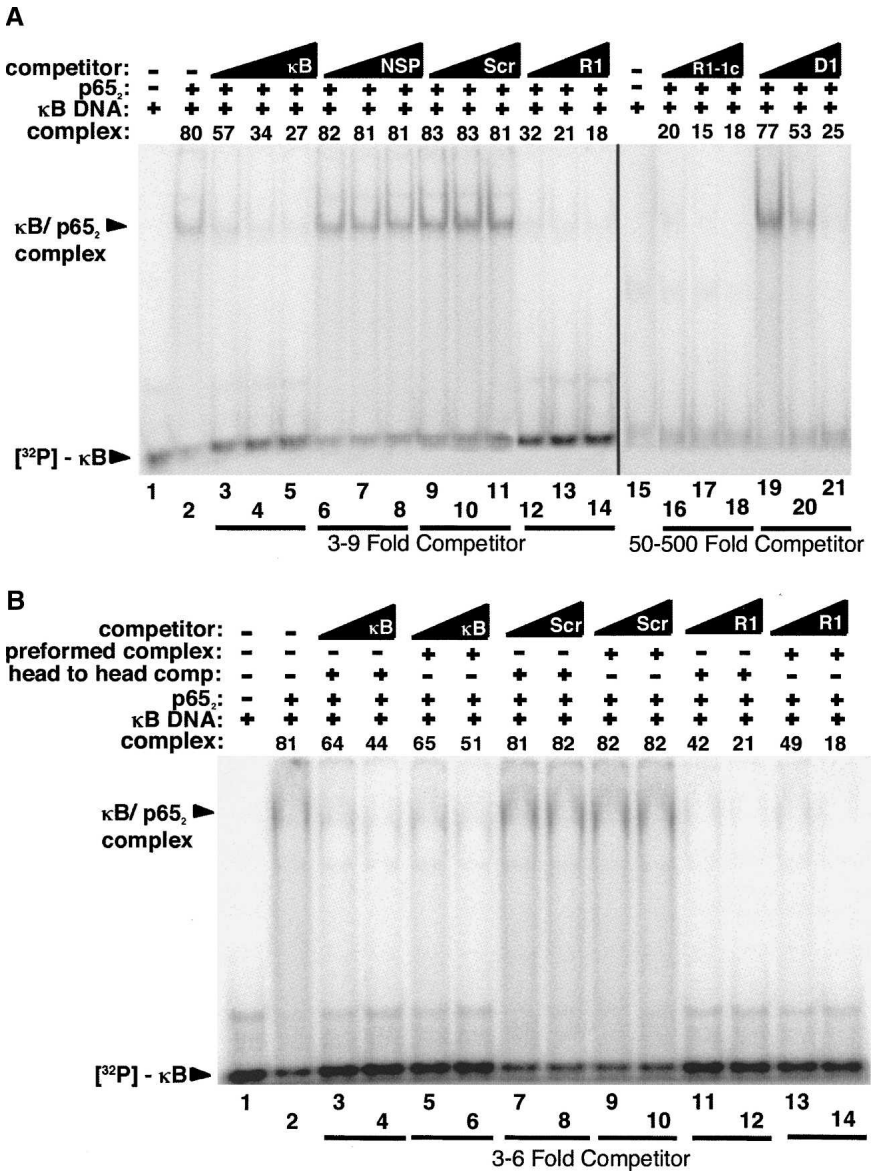

FIGURE 8. Anti-p65 RNAs R1 and D1 act as decoys for NF-κB. (*A*) Labeled κB DNA (1 nM) was incubated alone (lanes *1*,*15*) or in the presence of $p65_2$ (20 nM) alone (lane *2*) or together with various unlabeled competitors (lanes *3–14*,*16–21*): κB DNA (lanes *3–5*), nonspecific DNA (lanes *6–8*), scrambled RNA (lanes *9–11*), R1 RNA (lanes *12–14*), R1–1c RNA (lanes *16–18*), D1 RNA (lanes *19–21*). Triangles indicate increasing unlabeled competitor concentration (three-, six-, or ninefold molar excess [lanes *3–14*]) and (50-, 100-, or 500-fold molar excess [lanes *16–21*]) relative to $p65_2$ concentration. "Complex" indicates the percentage of radiolabeled probe shifted. (*B*) Labeled κB DNA (1 nM) was incubated alone (lanes *1*) in the presence of $p65_2$ (20 nM) alone (lane *2*) together with various unlabeled competitors in three- to sixfold molar excess in head-to-head competition (lanes *3–4*,*7–8*,*11–12*) or preincubated with $p65_2$ to obtain preformed DNA/ protein complexes with subsequent addition of various unlabeled competitors in three- to sixfold molar excess (lanes *5–6*,*9–10*,*13–14*). "Complex" indicates the percentage of radiolabeled probe shifted.

mutations were unsuccessful. Anti-p50 could easily be truncated to an imperfect hairpin of ~30 nt, whereas anti-p65 R1 cannot be truncated to fewer than 54 nt without significant loss of affinity for $p65_2$. Based on the complex noncanonical base pairing and stacking within the internal loop of anti-p50 (Huang et al. 2003; Reiter et al. 2008), we think it is likely that the internal loops of the anti-p65 aptamers described here also form complex structures. It is interesting to speculate that anti-p65 RNAs may also mimic features of the major groove of κB site DNA.

Because of the sequence similarity of p50 and p65 in the DNA-binding surface, we had anticipated that a small number of substitutions in anti-p50 could yield an anti-p65 aptamer. However, we show that no high-affinity p65-specific aptamer could be readily selected after 12 rounds of selection and complete convergence of the degenerate anti-p50 library to a single sequence. Interestingly, the resulting D1 aptamer has moderate affinity for both $p50_2$ and $p65_2$. D1 is also a potential therapeutic lead because of its ability to bind both subunits of the p50/p65 NF-κB heterodimer.

The NF-κB aptamers presented herein also provide us with the exciting prospect of optimizing $p65_2$ binding within a eukaryotic organism, such as *Saccharomyces cerevisiae*, as we have previously reported for anti-p50 (Cassiday and Maher 2001; Cassiday and Maher 2003). Another potential strategy involves selection of optimal RNA linker sequences to combine the p50 and p65 aptamers to form a heterodimeric aptamer that is competent for simultaneous binding of both subunits of NF-κB heterodimers. Heterodimeric aptamers may provide an ideal tool for studying the functional significance of heterodimer and homodimer populations of NF-κB protein.

MATERIALS AND METHODS

Oligonucleotides

DNA oligonucleotides were synthesized by phosphoramidite methodology in the Mayo Foundation Molecular Biology Core Facility. RNA transcripts were prepared by in vitro transcription using T7 RNA polymerase (Epicentre) from DNA templates created by PCR extension of overlapping primers. Synthetic DNA templates for in vitro transcription were either randomized (5′-GTGATATC$_3$T$_2$CGA$_2$-N$_{60}$-C$_3$AGCT$_2$AG$_2$CGAG-3′) or were based on degenerate anti-p50 (5′-CATGCAGTGTC

$TAT_2CTCGAGTAGC\mathit{GATC_2TGA_3CTGT_2ATA_2G_2T_2G_2C_2GATC}GCTAGCATGCA_2CTGACTCG_2ATA_2GC$-3′) with degeneracy indicated by italics. Phosphoramidite mixtures were adjusted to yield equal base incorporation at each position (random library) or 9% random mutagenesis at each position (degenerate library). DNA duplexes for competition electrophoretic mobility shift assays were prepared by annealing complementary DNA oligonucleotides in a 1:1 ratio in the presence of 200 mM NaCl. Duplex DNA was radiolabeled using the Klenow fragment of DNA polymerase I to fill the recessed 3′ termini in the presence of [α-^{32}P]-dATP and 2 mM dGTP, dTTP, and dCTP.

NF-κB protein expression and purification

One-liter cultures of *Escherichia coli* strain BL21(DE3) harboring a pET-11a plasmid derivative encoding human p50 were grown with shaking at 37°C to an A_{600} value of 0.6, then induced with 1 mM IPTG. After 3 h, cells were harvested, washed with sterile water, and frozen at −80°C. Pellets were resuspended in 30 mL buffer A (20 mM HEPES at pH 7.5, 0.4 M NaCl, 2 mM EDTA, 5% [v/v] glycerol, 1 mM DTT, 1 μg/μL pepstatin, 1 μg/μL leupeptin) and sonicated. Cell debris was pelleted, and polyethyleneimine (adjusted to neutral pH) was added to a final concentration of 0.1% (w/v) to precipitate nucleic acids. Saturated ammonium sulfate was then added to the supernatant to a final concentration of 55% (w/v), and the precipitated protein was collected by centrifugation at 14,000 rpm for 30 min. The resulting protein pellet was dissolved in 50 mL buffer B (20 mM HEPES at pH 7.5, 2 mM EDTA, 5% [v/v] glycerol, 1 mM DTT, 1 μg/μL pepstatin, 1 μg/μL leupeptin) and loaded onto a Hi-trap Sepharose column, which was washed and developed with a NaCl gradient. Fractions were monitored by SDS-PAGE, and peak fractions were pooled and concentrated. Protein was further purified using a Superdex-200 size exclusion column developed with buffer B plus 1 M NaCl. Peak fractions were stored in buffered 50% glycerol at −20°C. Purification of recombinant p65 protein was as for p50 except for the following modifications. After induction at an A_{600} value of 0.4 with 0.1 mM IPTG, cultures were grown overnight at room temperature. Cells were resuspended in buffer C (20 mM Tris-HCl at pH 8.0, 50 mM NaCl, 1 mM $MgCl_2$, 1 μg/μL pepstatin, 1 μg/μL leupeptin, 5% [v/v] glycerol, and 20 mM β-mercaptoethanol) and sonicated. The clarified lysate was passed over a SP-sepharose Fast Flow cation exchange column. The p65 protein (pI: 7.1) was present in the flow-through. This material was passed over a Q-sepharose anion exchange column, and p65 was again collected in the flow-through fraction. The protein was then loaded onto a mono S cation exchange column and eluted with a NaCl gradient of 50–200 mM at 4°C. Protein was then further purified using a Superdex-200 column, and peak fractions were stored in buffer C with 50% glycerol at −20°C.

Selection of RNAs that bind to $p65_2$

Initial DNA pools encoding random and degenerate RNAs were prepared by PCR amplification and transcribed by radiolabeling in vitro using T7 RNA polymerase (Epicentre). The initial selection round involved 366 pmol RNA library (∼2 transcripts each from $\sim 10^{14}$ DNA templates). RNAs were diluted to 37 nM in selection buffer (10 mM HEPES at pH 7.5, 100 mM NaCl, 1 mM DTT) and incubated with 6 nM $p65_2$ in a volume of 10 mL for 2 h with occasional mild agitation at 37°C. Mock selections without $p65_2$ were performed in parallel. RNAs were preincubated with 0.2 μm nitrocellulose filter strips in selection rounds 3–9 to remove RNAs with high affinity for nitrocellulose. Binding reactions were filtered through prewet nitrocellulose followed by washing with 5 mL of selection buffer. Bound RNAs were then eluted by incubating filters in 0.5 mL elution buffer (200 mM Tris-HCl at pH 7.6, 2.5 mM EDTA, 300 mM NaCl, 2% SDS) at 65°C for 35 min. RNAs were recovered by extraction with phenol:chloroform (1:1) and precipitation with ethanol. The yield of selected radiolabeled RNA at each round was monitored by Cerenkov counting of filters. Half of the selected RNAs were reverse transcribed using MMLV reverse transcriptase in preparation for the next round (Soukup et al. 1996). At various stages, PCR products were cloned and sequenced to monitor library diversity.

Cloning and sequencing

Double-stranded DNA products amplified after various selection rounds were cloned using the pGEM-T Easy vector (Promega) and sequenced in the Mayo Foundation Molecular Biology Core Facility. Predicted RNA secondary structures were determined using the Zuker Mulfold program (Jaeger et al. 1989, 1990; Zuker 1989).

Binding affinity estimates

RNA molecules were 3′ radiolabeled by incorporation of [^{32}P]-pCp in the presence of T4 RNA ligase. K_d estimates for binding of NF-κB proteins to radiolabeled RNA were obtained by incubating 1 nM RNA with protein (1 nM to 1 μM) in buffer (20 mM Tris-HCl at pH 8.0, 50 mM NaCl, 1 mM $MgCl_2$) followed by filtering over prewetted nitrocellulose filters, washing, and scintillation counting. Binding affinities were estimated by fitting the fractional saturation (θ) of the radiolabeled nucleic acid target to the total protein concentration (L) using Equation 1:

$$\theta = (L)/(K_d + L), \tag{1}$$

where K_d is the equilibrium dissociation constant.

Electrophoretic mobility shift experiments

The ability of various truncated RNAs to bind $p65_2$ protein was determined by incubating 1 nM radiolabeled RNA with various concentrations of $p65_2$ in 20 μL binding reactions containing 20 mM Tris-HCl (pH 8.0), 50 mM NaCl, 1 mM $MgCl_2$, 1 μg poly(dI·dC), 0.5 μg tRNA, 0.25 mg/mL BSA, 5% (v/v) glycerol, and 1 mM DTT. Binding reactions were incubated for 20 min at room temperature and electrophoresed through native polyacrylamide gels in 0.25× TBE buffer. Complexes were detected and analyzed by storage phosphorimaging.

Stoichiometry analysis of R1 RNA/$p65_2$ complexes

The stoichiometry of R1 RNA/ $p65_2$ complexes was investigated by incubating a constant concentration of $p65_2$ (50 nM) in 20 μL binding reactions (20 mM Tris-HCl at pH 8.0, 50 mM NaCl, 1 mM $MgCl_2$) together with increasing concentrations of [^{32}P]-pCp-labeled R1 RNA (0.1-, 0.25-, 0.5-, 1.0-, 1.5-, 2.0-, and 3.0-fold

molar excess relative to protein concentration). Components were incubated for 20 min and electrophoresed through native polyacrylamide gels in 0.25× TBE buffer. Complexes were detected and analyzed by storage phosphorimaging.

RNA structure analysis

RNA (~75 pmol) was dephosphorylated by calf intestinal alkaline phosphatase (New England Biolabs) and 5′-end labeled with T4 polynucleotide kinase and [γ-^{32}P]-ATP or 3′-end labeled with T4 RNA ligase and [^{32}P]-pCp. Radiolabeled RNA was purified by denaturing polyacrylamide gel electrophoresis. Partial alkaline hydrolysis ladders were prepared at pH 8.3, and G-specific ladders were created using RNase T_1 (Epicentre) at 52°C in the presence of urea, as described (McDonald and Maher 1995). For probing the presence of single-stranded RNA, mung bean nuclease (1 U, New England Biolabs) was added to RNA (~100,000 cpm) in 50 mM NaCl, 10 mM Tris-HCl, 10 mM $MgCl_2$, 1 mM DTT (pH 7.9) at 30°C for 1 min prior to addition of urea loading buffer and freezing on dry ice. For RNase V_1 (Ambion) treatment, RNAs were dissolved in Structure Buffer (10 mM Tris at pH 7, 100 mM KCl, 10 mM $MgCl_2$) and heated to 70°C for 5 min followed by cooling on ice. RNA samples (~100,000 cpm) were treated with 1 U of RNase V_1 for 15 min at room temperature in the presence of 5 μg of yeast RNA. After precipitation, RNAs were analyzed by electrophoresis on 10% denaturing polyacrylamide sequencing gels followed by storage phosphorimaging.

Competition binding assays

RNA/RNA and RNA/DNA competition for $p65_2$ binding was monitored by radiolabeling either an RNA molecule or a DNA duplex containing a κB site (bold): [5′-AGT_2GAG**G_3ACT_3C**$_2$ CAG_2C; top strand shown]. Binding reactions contained 20 mM Tris-HCl (pH 8.0), 50 mM NaCl, 1 mM $MgCl_2$, 1 μg poly(dI·dC), 0.5 μg tRNA, 0.25 μg/μL BSA, 1 mM DTT, 1 nM labeled DNA duplex, 10 nM $p65_2$, and varying ratios of unlabeled RNA or DNA competitors. Binding reactions were incubated at room temperature for 20 min, electrophoresed on 6% native polyacrylamide gels in 0.25× TBE buffer, and visualized by storage phosphorimaging.

ACKNOWLEDGMENTS

We thank Dr. Kasandra Riley as well as present and past members of the Maher laboratory for technical assistance and Heather Thompson for editorial suggestions. We thank Dr. Gourisankar Ghosh for the p65 protein expression vector and initial samples of recombinant protein. This work was supported by the Mayo Foundation and by NIH grant GM68128.

Received October 16, 2007; accepted February 18, 2008.

REFERENCES

Baeuerle, P.A. and Baltimore, D. 1996. NF-κB: Ten years after. *Cell* **87:** 13–20.

Baldwin Jr., A.S. 1996. The NF-κB and IκB proteins: New discoveries and insights. *Annu. Rev. Immunol.* **14:** 649–683.

Beg, A.A. and Baltimore, D. 1996. An essential role for NF-κB in preventing TNF-α-induced cell death. *Science* **274:** 782–784.

Brown, T.S. and Bevilacqua, P.C. 2005. Method for assigning double-stranded RNA structures. *Biotechniques* **38:** 368–372.

Burke, J.M. and Berzal-Herranz, A. 1993. In vitro selection and evolution of RNA: Applications for catalytic RNA, molecular recognition, and drug discovery. *FASEB J.* **7:** 106–112.

Burke, D.H., Scates, L., Andrews, K., and Gold, L. 1996. Bent pseudoknots and novel RNA inhibitors of type 1 human immunodeficiency virus (HIV-1) reverse transcriptase. *J. Mol. Biol.* **264:** 650–666.

Carmody, R.J., Ruan, Q., Palmer, S., Hilliard, B., and Chen, Y.H. 2007. Negative regulation of toll-like receptor signaling by NF-κB p50 ubiquitination blockade. *Science* **317:** 675–678.

Cassiday, L.A. and Maher III, L.J. 2001. In vivo recognition of an RNA aptamer by its transcription factor target. *Biochemistry* **40:** 2433–2438.

Cassiday, L.A. and Maher III, L.J. 2002. Having it both ways: Transcription factors that bind DNA and RNA. *Nucleic Acids Res.* **30:** 4118–4126. doi: 10.1093/nar/gkf512.

Cassiday, L.A. and Maher III, L.J. 2003. Yeast genetic selections to optimize RNA decoys for transcription factor NF-κB. *Proc. Natl. Acad. Sci.* **100:** 3930–3935.

Cassiday, L.A., Lebruska, L.L., Benson, L.M., Naylor, S., Owen, W.G., and Maher III, L.J. 2002. Binding stoichiometry of an RNA aptamer and its transcription factor target. *Anal. Biochem.* **306:** 290–297.

Chen, F.E. and Ghosh, G. 1999. Regulation of DNA binding by Rel/NF-κB transcription factors: Structural views. *Oncogene* **18:** 6845–6852.

Chen, Y.Q., Ghosh, S., and Ghosh, G. 1998. A novel DNA recognition mode by the NF-κB p65 homodimer. *Nat. Struct. Biol.* **5:** 67–73.

Choi, K.H., Park, M.W., Lee, S.Y., Jeon, M.Y., Kim, M.Y., Lee, H.K., Yu, J., Kim, H.J., Han, K., Lee, H., et al. 2006. Intracellular expression of the T-cell factor-1 RNA aptamer as an intramer. *Mol. Cancer Ther.* **5:** 2428–2434.

Dobrovolskaia, M.A. and Kozlov, S.V. 2005. Inflammation and cancer: When NF-κB amalgamates the perilous partnership. *Curr. Cancer Drug Targets* **5:** 325–344.

Dutta, J., Fan, Y., Gupta, N., Fan, G., and Gelinas, C. 2006. Current insights into the regulation of programmed cell death by NF-κB. *Oncogene* **25:** 6800–6816.

Ellington, A.D. and Szostak, J.W. 1990. In vitro selection of RNA molecules that bind specific ligands. *Nature* **346:** 818–822.

Escarcega, R.O., Fuentes-Alexandro, S., Garcia-Carrasco, M., Gatica, A., and Zamora, A. 2007. The transcription factor nuclear factor-κB and cancer. *Clin. Oncol. (R Coll Radiol)* **19:** 154–161.

Fujita, T., Nolan, G., Ghosh, S., and Baltimore, D. 1992. Independent modes of transcriptional activation by the p50 and p65 subunits of NF-κB. *Genes & Dev.* **6:** 775–781.

Garg, A. and Aggarwal, B.B. 2002. Nuclear transcription factor-κB as a target for cancer drug development. *Leukemia* **16:** 1053–1068.

Ghosh, G., van Duyne, G., Ghosh, S., and Sigler, P.B. 1995. Structure of NF-κB p50 homodimer bound to a κB site. *Nature* **373:** 303–310.

Guo, J., Verma, U.N., Gaynor, R.B., Frenkel, E.P., and Becerra, C.R. 2004. Enhanced chemosensitivity to irinotecan by RNA interference-mediated down-regulation of the nuclear factor-κB p65 subunit. *Clin. Cancer Res.* **10:** 3333–3341.

Hayden, M.S. and Ghosh, S. 2004. Signaling to NF-κB. *Genes & Dev.* **18:** 2195–2224.

Huang, D.B., Vu, D., Cassiday, L.A., Zimmerman, J.M., Maher 3rd, L.J., and Ghosh, G. 2003. Crystal structure of NF-κB (p50)2 complexed to a high-affinity RNA aptamer. *Proc. Natl. Acad. Sci.* **100:** 9268–9273.

Jaeger, J.A., Turner, D.H., and Zuker, M. 1989. Improved predictions of secondary structures for RNA. *Proc. Natl. Acad. Sci.* **86:** 7706–7710.

Jaeger, J.A., Turner, D.H., and Zuker, M. 1990. Predicting optimal and suboptimal secondary structure for RNA. *Methods Enzymol.* **183:** 281–306.

Karin, M. 2006. Nuclear factor-κB in cancer development and progression. *Nature* **441:** 431–436.

Karin, M. and Greten, F.R. 2005. NF-κB: Linking inflammation and immunity to cancer development and progression. *Nat. Rev. Immunol.* **5:** 749–759.

Karin, M. and Lin, A. 2002. NF-κB at the crossroads of life and death. *Nat. Immunol.* **3:** 221–227.

Karin, M., Cao, Y., Greten, F.R., and Li, Z.W. 2002. NF-κB in cancer: From innocent bystander to major culprit. *Nat. Rev. Cancer* **2:** 301–310.

Kitajima, I., Shinohara, T., Bilakovics, J., Brown, D.A., Xu, X., and Nerenberg, M. 1992. Ablation of transplanted HTLV-I *tax*-transformed tumors in mice by antisense inhibition of NF-κB. *Science* **258:** 1792–1795.

Lebruska, L.L. and Maher III., L.J. 1999. Selection and characterization of an RNA decoy for transcription factor NF-κB. *Biochemistry* **38:** 3168–3174.

Lin, A. and Karin, M. 2003. NF-κB in cancer: A marked target. *Semin. Cancer Biol.* **13:** 107–114.

Mayo, M.W., Wang, C.-Y., Cogswell, P.C., Rogers-Graham, K.S., Lowe, S.W., Der, C.J., and Baldwin, A.S. 1997. Requirement of NF-κB activation to suppress p53-independent apoptosis induced by oncogenic Ras. *Science* **278:** 1812–1815.

McDonald, C.D. and Maher III., L.J. 1995. Recognition of duplex DNA by RNA polynucleotides. *Nucleic Acids Res.* **23:** 500–506. doi: 10.1093/nar/23.3.500.

Mi, J., Zhang, X., Rabbani, Z.N., Liu, Y., Su, Z., Vujaskovic, Z., Kontos, C.D., Sullenger, B.A., and Clary, B.M. 2006. H1 RNA polymerase III promoter-driven expression of an RNA aptamer leads to high-level inhibition of intracellular protein activity. *Nucleic Acids Res.* **34:** 3577–3584. doi: 10.1093/nar/gkl482.

Nakanishi, C. and Toi, M. 2005. Nuclear factor-κB inhibitors as sensitizers to anticancer drugs. *Nat. Rev. Cancer* **5:** 297–309.

Perwez Hussain, S. and Harris, C.C. 2007. Inflammation and cancer: An ancient link with novel potentials. *Int. J. Cancer* **121:** 2373–2380.

Reiter, N.J., Maher III, L.J., and Butcher, S.E. 2008. DNA mimicry by a high-affinity anti-NF-κB RNA aptamer. *Nucleic Acids Res.* **36:** 1227–1236. doi: 10.1093/nar/gkm1141.

Soukup, G.A., Ellington, A.D., and Maher III., L.J. 1996. Selection of RNAs that bind to duplex DNA at neutral pH. *J. Mol. Biol.* **259:** 216–228.

Suzan, M., Salaun, D., Neuveut, C., Spire, B., Hirsch, I., Le Bouteiller, P., Querat, G., and Sire, J. 1991. Induction of NF-KB during monocyte differentiation by HIV type 1 infection. *J. Immunol.* **146:** 377–383.

Tuerk, C. and Gold, L. 1990. Systematic evolution of ligands by exponential enrichment: RNA ligands to bacteriophage T4 DNA polymerase. *Science* **249:** 505–510.

Van Waes, C. 2007. Nuclear factor-κB in development, prevention, and therapy of cancer. *Clin. Cancer Res.* **13:** 1076–1082.

Verma, I.M., Stevenson, J.K., Schwarz, E.M., Van Antwerp, D., and Miyamoto, S. 1995. Rel/NF-κB/IκB family: Intimate tales of association and dissociation. *Genes & Dev.* **9:** 2723–2735.

Zhao, X., Shi, H., Sevilimedu, A., Liachko, N., Nelson, H.C., and Lis, J.T. 2006. An RNA aptamer that interferes with the DNA binding of the HSF transcription activator. *Nucleic Acids Res.* **34:** 3755–3761. doi: 10.1093/nar/gkl470.

Zuker, M. 1989. On finding all suboptimal foldings of an RNA molecule. *Science* **244:** 48–52.